Chapter 9

PLUME-IN-GRID TREATMENT OF MAJOR POINT SOURCE EMISSIONS

N. V. Gillani
Earth System Science Laboratory
University of Alabama in Huntsville
Huntsville, Alabama 35899

James M. Godowitch*
Atmospheric Modeling Division
National Exposure Research Laboratory
U.S. Environmental Protection Agency
Research Triangle Park, North Carolina 27711

ABSTRACT

A plume-in-grid (PinG) technique has been developed to more realistically treat the dynamic and chemical processes impacting selected, major point source pollutant plumes in the Community Multiscale Air Quality (CMAQ) modeling system. The principal science algorithms include a Plume Dynamics Model (PDM) and a Lagrangian reactive plume code. The PDM processor simulates plume rise, horizontal and vertical plume growth, and transport of each plume section during the subgrid scale phase. It generates a data file of this information for use by the PinG module. In contrast to the traditional Eulerian grid modeling method of instantly mixing the emissions from each point source into an entire grid cell volume, the PinG module simulates the relevant physical and chemical processes during a subgrid scale phase which allows each plume section to expand in a realistic manner and to evolve chemically. The PinG module is fully integrated into the CMAQ Chemical Transport Model (CCTM) in order to utilize the grid concentrations as boundary conditions and it provides a feedback of the plume pollutants to the grid model concentration field at the proper time and grid location. The technical approaches and the model formulation of the relevant processes treated by this plume-in-grid approach are described. The capabilities and limitations of the initial version of PinG are also discussed and selected results from a test application for a single point source are briefly described.

*On assignment from the National Oceanic and Atmospheric Administration, U.S. Department of Commerce. Corresponding author address: James M. Godowitch, MD-80, Research Triangle Park, NC 27711. E-mail: jug@hpcc.epa.gov

9.0 PLUME-IN-GRID TREATMENT OF MAJOR POINT SOURCE EMISSIONS

9.1 Introduction

Significant emissions of anthropogenic nitrogen oxides (NO_x) and sulfur oxides (SO_x) are released from individual elevated point sources into the atmosphere at various levels. These major point source emissions are distributed throughout the U.S. The physical dimensions of their plumes are relatively small initially and expand at finite growth rates. This diffusion-limited nature of plumes is in sharp contrast to the traditional method applied in Eulerian photochemical grid modeling, which has been to uniformly and instantly mix point source emissions into the entire volume of a model grid cell. Depending on the meteorological conditions, however, pollutant plumes may require up to several hours to grow to the typical size of a regional model grid cell. Since the horizontal grid resolution of regional scale domains for Eulerian models has generally been 20-30 km or greater, a real-world pollutant plume may remain a subgrid scale feature at current regional model grid resolutions for a substantial time period and considerable distance after release. Thus, the widely-used grid modeling approach inadequately treats subgrid scale plume transport and diffusion.

There are also important implications on the chemical processes in models due to the inability of large grid cells to adequately resolve a major point source plume. As a real-world plume gradually grows, it concurrently evolves chemically as it entrains surrounding ambient air often richer in volatile organic compounds (VOCs). However, these dynamic and chemical processes of plumes are neglected when large point source emissions are instantly diluted into large grid cells with other anthropogenic area emissions, which may actually be separated spatially from a plume. The effect is that the simultaneous availability of NO_x and VOC's in a large grid cell prematurely initiates rapid photochemistry leading to distortion in the spatial and temporal features of secondary species concentrations. This overdilution of point source emissions and the subsequent distortion of chemical processes contribute to model uncertainty. Consequently, it has been recognized that a realistic, subgrid scale modeling approach is needed which simulates the relevant physical and chemical processes impacting this notable class of large point source emissions, and in particular, that has the capability of properly resolving the spatial scale of plumes and their growth.

There are approaches which have been applied in attempts to resolve fine scale emissions in regional grid models. These have included uniform, nested grid modeling (Odman and Russell, 1991; Chang et al., 1993), non-uniform grid modeling (Mathur et al., 1992), and the plume-in-grid modeling (PinG) technique. The nested grid (telescoping) modeling approach employs the same Eulerian model and simulations are performed with progressively finer-mesh grid sizes within a domain to better resolve small scale emission features. While an advantage of this approach is the use of a single model algorithm, a disadvantage is the successively higher computational burden as the grid cell size is reduced in order to resolve major emission sources. Efforts to implement and apply the plume-in-grid technique, in particular, have been performed by Seigneur et al. (1983) in a version of the Urban Airshed Model (UAM-PARIS), by Morris et al. (1992) in the UAM-V model, by Kumar and Russell (1996) in the Urban-Regional Model

(URM), and by Myer et al. (1996) in the SAQM (SARMAP Air Quality Model) model. Briefly, each of these PinG efforts simulate multiple plumes or puffs in a domain with no interaction between individual plumes. Seigneur et al. (1983) employed a rectangular plume cross-section divided into vertically well-mixed plume cells exhibiting varying widths to maintain equal pollutant mass among the cells. It was applied to an urban domain with a 4 km grid cell size. The other efforts employ an elliptical plume section divided into concentric rings, except for the Kumar and Russell (1996) PinG. Plume material in an outermost elliptic ring or shell is sequentially transferred to the grid model as it attains the grid size. In the treatment by Kumar and Russell, the plume was returned to the grid model after one hour. The general result of applications from these PinG implementations was that noticeable differences were found primarily within or near the grid cells containing the major point sources and negligible impact was found far downwind. This finding is to be expected since these formulations seemed to focus on the plume-core chemistry only in an early phase of plume chemical evolution with the feedback of plume pollutants occurring rather quickly to the grid model.

A cooperative research and development effort was undertaken to design and implement a plume-in-grid (PinG) capability in the Models-3 CMAQ Chemical Transport Model (CCTM) in order to address the need for an improved approach to treat major point source emissions. The current PinG approach has been designed to be suitable for the largest, isolated point source emissions with grid resolutions of regional modeling domains, where the subgrid scale error in the representation of these sources is expected to be greatest without a PinG treatment. An important consideration is to be able to spatially resolve a pollutant plume and to adequately simulate physical expansion so that the chemical evolution can occur gradually. Therefore, the objectives with this PinG technique are to provide an improved characterization of the near-source pollutant field from the subgrid scale plume concentrations and to also generate better regional pollutant concentrations downwind due to the feedback of the PinG concentrations to the gridded domain. Consequently, when the PinG approach is applied to the largest point source emissions in a regional, coarse-grid domain, improved initial and boundary conditions are anticipated for use with subsequent simulations for a subdomain of the same grid resolution or for fine-mesh nested domains that also need the regional gridded concentration fields.

In this chapter, the conceptual design of the PinG approach is discussed. The key modeling components are a Plume Dynamics Model (PDM) and a Lagrangian reactive plume model designated as the PinG module since it is fully integrated and coupled with the CCTM Eulerian grid model. The PDM has been developed to serve as a processor program to generate plume dimensions, plume position information and related parameters needed by the PinG module. The descriptions of the mathematical formulations and numerical techniques contained in these modeling components are also presented. Their solutions form the basis of the physical-chemical simulations of subgrid scale plumes as implemented in the principal algorithms of the PinG modeling components.

9.2 Overview of the Conceptual Framework of the Plume-in-Grid Treatment

The PinG technique is intended for the largest point sources, designated as major elevated point source emissions (MEPSEs), which are isolated from notable area emission sources. A complete description of the various criteria available to classify a point source as a MEPSE is provided in the emission processing system in chapter 4. In the context of photochemical modeling, the NO_x emission rate is a useful criterion to classify a major point source as a MEPSE from the thousands of individual major point sources in an inventory. Based on a NO_x emission rate criterion of 50 tons/day as a lower limit, Figure 9-1 depicts the group of fewer than 100 MEPSEs in a 36 km gridded domain covering the eastern US with emission rates greater than this criterion. The MEPSE sources are situated away from major metropolitan emission source areas. It reveals that numerous MEPSEs are distributed throughout the Ohio River and Tennessee River valley regions. Since the current PinG technique also relies on linear superposition of MEPSE plumes for determining the impact on grid concentration, the relatively isolated MEPSEs located in these remote rural environments also provide for the lowest likelihood of plume-plume interactions.

An important feature of a PinG treatment is that it must be able to reproduce the various stages in the chemical evolution found in a large, rural point source plume. Based on daytime experimental field study plume data, Gillani and Wilson (1980) documented three distinct stages, as displayed in Figure 9-2, in the chemical evolution of ozone (O_3) in a pollutant plume from a high NO_x source. The O_3 data measured across a plume at different downwind distances in Figure 9-2 illustrate ozone evolution in a large NO_x point source plume. Although NO_x was not obtained, it would display a similar variation to SO_2 shown in Figure 9-2. During the first stage, the relatively fresh plume is dominated by primary NO_x emissions and an O_3 deficit exists in the plume due to titration by very high NO concentrations. The chemistry in stage 1 is mostly inorganic and VOC-limited since MEPSE plumes generally exhibit low VOC emissions. The second stage represents a transition in the chemistry with rapid production of O_3 along the plume edges and some O_3 recovery in the plume core. Plume growth from dispersion processes allows for entrainment of background air which generally contains a richer supply of ambient VOC concentrations. Consequently, this promotes rapid photochemical O_3 production which leads to the characteristically higher O_3 concentrations observed at the edges of a plume during this stage. Figure 9-2 reveals that stage 2 certainly exhibits considerable subgrid scale plume structure in species concentrations. Therefore, the proper simulation of plume chemistry throughout stage 2 is a key phase for a realistic, overall characterization of plume chemical evolution. In fact, full completion of stage 2 is an important requirement for a chemical criterion during the PinG simulation before the plume pollutants are transferred to the grid system. In stage 3, the plume is chemically mature and substantially diluted. In this mature stage, the broad plume would also exhibit a high VOC/NO_x ratio, low NO_x concentrations, and O_3 concentrations in excess of background levels. In the modeling system, background (boundary) concentrations are provided from a CCTM grid cell containing the subgrid scale plume section.

The chemical evolution, as described above, for a large MEPSE plume in the eastern US generally may take up to several hours to reach full maturity even during the daytime period. The photochemical cycle is strongly influenced by the plume growth rate, particularly the rate of

horizontal spread, with stage 3 achieved when a typical MEPSE plume attains a width of about 30 km during the daytime period. In addition, the time period to reach chemical maturity is also a function of the emission rate. There is a range of emission rates even within a MEPSE group. For example, particular MEPSE plume with lower NO_x emissions is expected to exhibit a faster chemical evolution than a MEPSE with a higher emission rate, assuming other factors being the same. Nevertheless, during the subgrid scale simulation period, the plume may travel a considerable distance downwind (i.e. several model grid cells) of its source location in the daytime planetary boundary layer (PBL) during the summer before reaching a width comparable to the grid cell size.

The conceptual design of the Models-3 PinG is illustrated in Figure 9-3. PinG components simulate the relevant processes impacting the hourly emission rate of all pollutant species during the subgrid scale phase and it provides a feedback, or "handover", of the modeled plume species concentrations at an appropriate handover time ($t_{H/O}$) to the CCTM grid framework. The PinG module operates in a Lagrangian modeling framework to simulate the dynamics and kinetics in a moving plume section during the subgrid scale phase whose duration depends primarily upon source strength, plume growth rate, chemical composition of the background CCTM grid concentrations, and sunlight. The PinG module simulates the plume processes concurrently during the simulation of the CCTM grid model.

The PinG module contains a series of rectangular plume cross-sections, each of which are composed of a contiguous, crosswind array of plume cells with the depth of each cell extending vertically from plume bottom to a top height. As displayed in Figure 9-3a, the vertical depth of the single-layer plume model may be elevated initially, however, it eventually extends from the surface to the PBL height (z_i). This one-layer plume structure in the initial PinG module also presents a limitation under high wind speed shear conditions since this situation cannot be modeled adequately. While strong speed shears are more frequent during the nocturnal period, the vertical extent of a plume is also generally confined, which lessens the possible impact of speed shear. Nevertheless, this condition is identified and appropriately handled by the PinG components.

9.3 Formulation of the Plume-in-Grid Modeling Components

9.3.1 Description of the Plume Dynamics Model

The PDM was developed to serve as a processor program in order to provide data needed for the CCTM/PinG simulation. Therefore, the PDM and the PinG module are closely linked through the PDM data file. The key processes simulated by the PDM include plume rise, plume transport, and plume dispersion of each MEPSE plume cross-section. The PDM also specifies when a particular plume section is to be transferred to the grid model based on an indicator flag which communicates to the PinG module when this process is to be performed. The PDM is capable of simultaneously treating up to 100 MEPSEs in a single simulation with the impact on computational time a function of the number of MEPSEs simulated. In addition, the maximum

simulation period is currently limited to 24 hours. Therefore, a single simulation of the CCTM with PinG is also limited to a 24-hour time period.

9.3.1.1 Aspects of Plume Rise of MEPSE Sources

The plume rise treatment implemented in PDM contains the same algorithms applied in the Emissions-Chemistry Interface Processor (ECIP). A detailed discussion of the plume rise equations and treatment has been provided in section 4.4.2 of chapter 4 on the MEPPS system and therefore is not repeated herein.

The plume rise algorithms handle the entire diurnal cycle since plume sections are released hourly throughout the 24 hour cycle. The temporal variation of the final effective plume height for hourly MEPSE plume releases is illustrated in Figure 9-4. In this case, a diurnal variation in the final plume height is evident with lower plume rise occurring at night believed to be due in part to stronger wind speeds. The plume height increases during the morning period as the PBL height grows and the relatively high values found in the afternoon display little variation until the end of the daytime period.

A notable feature of MEPSE plumes also revealed in Figure 9-4 is the rather significant height often attained by this class of point sources. Statistics of the stack parameters from MEPSE and non-MEPSE groups of major point sources were determined. A comparison indicates notable differences in certain stack parameters between these source groups. The average values from a MEPSE group containing 84 stacks compared to the other major point source class containing 6539 stacks show a stack height of 207 m versus 45 m , a stack velocity of 20 m/s versus 12.5 m/s , a stack diameter of 7.5 m versus 2.3 m, a stack exit temperature of 410^o K versus 424^o K, and a stack exit flow rate of 908 m^3/s versus 105 m^3/s, respectively. Clearly, these results indicate why MEPSE plume heights attain higher levels than most point sources. In general, MEPSE stacks are considerably higher and their plumes exhibit greater buoyancy flux due primarily to greater physical dimensions which contribute to higher plume rise heights.

9.3.1.2 Plume Dispersion Methods

A key aspect of modeling a subgrid scale reactive plume, as noted earlier, is the importance of realistically specifying plume dimensions during travel time downwind. Practical methods have been applied in the initial version of PDM to determine the horizontal and vertical dimensions of each Lagrangian plume section throughout its life cycle.

Each rectangular plume cross-section has a width (W_p) and an overall height from plume bottom to top denoted by H_p . The traditional dispersion parameters in the horizontal (σ_y) and vertical (σ_z) have been employed in order to derive these plume dimensions. In the current version, the plume width and plume height values are determined according to

$$W_p = \boldsymbol{a}\sigma_y \qquad \text{(9-1a)}$$

where **a** has been set to 3.545 which is obtained from $2(\pi)^{½}$, an adjustment parameter from an elliptical shape to the rectangular plume. The top and bottom heights of each plume cross-

$$H_p = h_T - h_b \quad (9\text{-}1b)$$

section are denoted by h_T and h_b , respectively. The methods used to determine values for the parameters in Equations 9-1a and 9-1b are discussed next.

During the plume rise phase, a plume experiences initial growth due to buoyancy-induced turbulence. To account for this process, practical methods have been used to determine initial values for the dispersion parameters. The initial value of σ_y is computed according an expression suggested in Irwin (1979), as advanced by Pasquill (1976), given by

$$\sigma_{yo} = \Delta h/3.5 \quad (9\text{-}2)$$

In Equation 9-2, the initial value is a function of the plume rise (Δh) above the stack top.

Two methods have been installed to prescribe an initial vertical plume thickness. The widely used approach advanced by Briggs (1975) is to define H_p to be equivalent to the amount of plume rise (Δh). This method can result in a rather thick plume when there is considerable plume rise, particularly, at night when experimental evidence suggests nocturnal plumes may be relatively thin. Consequently, an optional approach provided as an experimental alternative has been included. It consists of an empirical form developed by Gillani (1996) which is based on analyses of observed plume data taken during a field study (Gillani et al., 1981). His regression analyses produced an expression given by

$$\sigma_{zo} = Ae^{(-BdT/dz)} \quad (9\text{-}3)$$

where dT/dz is the vertical ambient temperature gradient at the plume centerline height and the best-fit values for A and B are 15 and 117, respectively. A minimum σ_{zo} value is set to 3 m. Then, the initial H_p is determined from SZ0FA times $\sigma_{zo.}$ SZ0FA is a user-specified input parameter for a PDM simulation and it is currently set to 3.545.

Atmospheric turbulence and wind direction shear contribute to lateral plume growth during travel downwind. During the daytime convective period, the turbulence component is often dominant, although directional shear across the PBL also has an important role in contributing to plume spread with travel distance. In contrast, turbulence is generally weak at night, and horizontal

plume expansion may be dominated by wind direction shear over a plume's depth. Thus, the composite horizontal (lateral) dispersion parameter (σ_y) can be defined by

$$\sigma_y^2 = \sigma_{yt}^2 + \sigma_{ys}^2 + \sigma_{yo}^2 \quad (9\text{-}4)$$

where the turbulence (σ_{yt}) and direction shear (σ_s) terms may both contribute to horizontal plume growth after the initial plume spread.

A general form for σ_{yt} can be expressed by

$$\sigma_{yt} = \sigma_v T f(T/\tau_L) \quad (9\text{-}5)$$

where σ_v is the standard deviation of the lateral wind (v) component, T is travel time, and τ_L is the Lagrangian time scale. Although various expressions for the function, $f(t/\tau_L)$, have emerged (e.g., Draxler, 1976; Irwin, 1983), the following form from Weil (1985;1988) and applied by others (eg.,Venkatram, 1988) has been adopted.

$$f = \frac{1}{(1 + T/2\tau_L)^{1/2}} \quad (9\text{-}6)$$

This form is advantageous since it fits dispersion at both the short ($t < \tau_L$) and also long travel times ($t>>\tau_L$). Since the Lagrangian time scale is small relative to the plume section travel times which are often several hours, the expressions above reveal the familiar relation that σ_{yt} increases with the square root of travel time. Therefore, the following form according to Weil (1988) at long travel times, which has been examined by Clarke et al. (1983), is given by

$$\sigma_{yt}^2 = 2\sigma_v^2 \tau_L T \quad (9\text{-}7)$$

The above equation also displays the square root of time increase for the lateral dispersion parameter. Using modeled meteorological parameters from data files generated by MCIP, methods have been incorporated to determine the key parameters needed to solve the above expressions for σ_{yt}. Values for σ_v and τ_L are computed with a set of formulas presented in Hanna et al. (1982) and Hanna (1984), respectively, for various stability conditions based on Monin-Obhukov length (L) limits. For unstable conditions with $L < 0$

$$\sigma_v = u_*(12 - 0.5z_i/L)^{1/3} \quad (9\text{-}8)$$

$$\tau_L = 0.15z_i/\sigma_v \quad (9\text{-}9)$$

where z_i is the PBL height and u_* is the surface friction velocity. Under stable conditions defined by L > 0,

$$\sigma_v = 1.3u_*(1 - z/z_i) \quad (9\text{-}10)$$

$$\tau_L = 0.07z_i/\sigma_v(z/z_i)^{0.5} \quad (9\text{-}11)$$

and z is the height of the plume centerline. For neutral conditions (L = 0), values are determined by

$$\sigma_v = 1.3e^{(-2fz/u_*)} \quad (9\text{-}12)$$

$$\tau_L = 0.5z/\sigma_v(1 + 15fz/u_*) \quad (9\text{-}13)$$

where f is the Coriolis parameter. Using σ_v and τ_L values, the contribution from the turbulence component is computed incrementally from the derivative of Equation 9-7 and solved at each time step. The turbulence term is accumulated with time. Other semi-empirical methods available in PDM provide an alternative set of parameterizations for σ_v as provided by Weil (1988), Nieuwstadt(1984), and Arya(1984) for the different stability regimes, which may be selected from an input option when exercising PDM.

Wind direction shear due to turning of the wind over the vertical extent of a plume can also provide an important contribution to horizontal plume growth. While turbulence often dominates in the daytime PBL, direction shear during the nocturnal period is the principal mechanism for lateral plume expansion since turbulence is generally weak. An expression by Pasquill (1979) has been applied for all conditions to derive the direction shear term and is given by

$$\sigma_{ys}^2 = \alpha\Delta\theta^2X^2 \quad (9\text{-}14)$$

where α is 0.03, X is distance traveled by a plume section over a particular time interval, and $\Delta\theta$ is the wind direction difference (radians) over the vertical extent of the plume. The shear and turbulence terms are combined to solve for the total σ_y^2 in Equation 9-4.

After the initial plume thickness has been determined, the treatment for σ_z differs based on whether the plume height is above or below the PBL height. When the plume centerline height is above z_i, then the following expression from Gillani (1996) is applied to determine σ_z.

$$\sigma_z^2 = \sigma_{zo}^2 \frac{(1 + bT^{0.5})}{(1 + bT_o^{0.5})} \tag{9-15}$$

where b is 2.3 and T is travel time. Equation 9-15 is applied for T < 4 hours. At longer travel times, σ_z is set to zero for plumes existing above the PBL in the free atmosphere.

When a plume section is inside the PBL, the parameterization for the vertical plume dispersion parameter can be expressed by the same general form as σ_{yt}.

$$\sigma_z = \sigma_w \; T \; f(T/\tau_{Lz}) \tag{9-16}$$

As before, T is the travel time, and f has the same functional form as used for σ_{yt} although it now contains the Lagrangian time scale in the vertical (τ_{Lz}). The standard deviation of the vertical wind component (σ_w) is computed from the following expressions as given by Weil (1988) for unstable conditions and from Venkatram et al (1984) for neutral/stable conditions, respectively.

$$\sigma_w = 0.6w_* \qquad (convective\ \ case) \tag{9-17}$$

$$\sigma_w = 1.3u_*(1 - z/z_i)^{3/4} \qquad neutral/stable \tag{9-18}$$

The MCIP data files provide values for the fraction velocity (u_*), the convective velocity scale (w_*) and z_i. The plume centerline height is represented by z. The value of τ_{Lz} is computed from the following expressions by Hanna et al. (1982) for unstable and by Venkatram et al. (1984) for neutral/stable conditions.

$$\tau_{Lz} = 0.15\frac{z_i}{\sigma_w}\,[1 - e^{-5z/z_i}] \qquad (unstable) \tag{9-19}$$

In the latter expression, the length scale (l) is derived according to Venkatram et al. (1984).

An example application of these methods from a PDM simulation for a plume released at night from a MEPSE tall stack is shown in Figure 9-5. It shows the plume remains rather narrow and it

$$\tau_{Lz} = \frac{l}{\sigma_w} \qquad (neutral/stable) \tag{9-20}$$

stays elevated during the night. However, once the PBL grows beyond the plume height during the morning period, the plume thickness expands to fill the entire PBL with the plume top height matching z_i until it reaches a maximum height. The temporal variation of the plume width for the same example case is displayed in Figure 9-6. It shows that since the plume has a limited vertical extent at night, the plume width increases at a relatively slow rate as sufficient direction shear existed over the plume depth to cause lateral spreading. During the daytime, however, horizontal plume expansion occurs at a faster rate due to both greater turbulence and shear contributions. For a regional grid cell size of 36 km, the plume width for this release reached the physical grid size during the mid-morning hour. These results and other simulation results obtained from a daytime release versus observed values (Godowitch et al., 1995) provide preliminary evidence that these methods give a realistic depiction of the temporal behavior of the magnitudes of plume width and depth. Additional cases have also been exercised, although results are not shown herein, in order to assess the robustness and capability of the algorithms for different days. An extensive evaluation of these dispersion methods in PDM is planned against field study data obtained in the vicinity of major point sources in the Nashville, Tennessee area during the Southern Oxidant Study experimental period in the summer of 1995.

9.3.1.3 Plume Transport

With the updated plume top and bottom heights, the mean wind components are determined by averaging the winds over the layers spanned by the plume from h_b to h_T. This approach is currently applicable because of the single vertical layer structure of the current PinG module. The mean plume transport speed is used to determine an updated plume centerline position over the time interval. In addition, the positions of the plume edges at the bottom and top are also found in order to derive grid indices for later use in applying the proper grid cell concentrations for boundary conditions of each plume section.

9.3.2 Formulation of the Plume-in-Grid Module

9.3.2.1 Overview of the Plume Conceptual Framework

The Lagrangian plume model described originally by Gillani (1986) provided the conceptual basis for the Models-3 PinG module. However, the computer algorithms in the CCTM/ PinG

have been rewritten to contain updated methods for the key processes to be described in a later section.

In a modeling framework, a PinG plume cross-section can be described as a semi-infinite vertical slab moving along a Lagrangian trajectory with a mean wind flow. A plume cross-section is considered rectangular with a vertical height (H_p) and a width (W_p). Temporally, plume spread in the vertical and horizontal is specified by growth rates dH_p/dt and dW_p/dt, respectively. A plume cross-section is discretized laterally into an array of attached plume cells or pillars with the same H_p at time t, as depicted in Figure 9-7. Each plume section consists of N plume cells (currently, N = 10) with the width of each cell being equal. With respect to the plume centerline, there are N_L cells on the left side and N_R cells to the right side, such that

$$\begin{aligned} W_p &= \sum_{i=1}^{N_L} w_{Li} + \sum_{i=1}^{N_R} w_{Ri} \\ N &= N_L + N_R \end{aligned} \tag{9-21}$$

Currently, $N_L = N_R$ as L and R refer to the cells on the left and right sides, respectively. With respect to the plume centerline, the right side of the plume section expands to the right and the left side expands to the left. The width (w_i) of each plume cell is given by

$$(w_i)_{L/R} = (y_{i+1} - y_i)_{L/R} \tag{9-22}$$

where y values represent distances from the plume centerline position. Normalization of the plume cell widths is performed such that as the plume expands laterally, each cell width increases in the same proportion as the overall plume width. Thus, since the individual cell width is normalized with respect to the total plume width, the result is a transformed moving crosswind gridded array which is invariant with respect to time. The transformed crosswind coordinate (η) of the model is given by

$$\eta_i = \frac{y_i}{W_p} \tag{9-23}$$

and $d\eta_i/dt$ is zero. Therefore, although W_p and y_i are time dependent, η_i remains constant during a simulation. Additionally, although the fractional width of the cells across the plume section in the PinG has been prescribed to be equal in the current setup of the module, the algorithms have been generalized to allow for unequal plume cell widths and a different number of cells on the left and right sides of the plume centerline as described in Gillani (1986).

9.3.2.2 Formulation of the Plume Mass Balance Equation

The relevant processes, as noted in Figure 9-7, have been incorporated into the plume equation for the mass balance of individual species. They include dilution and entrainment due to vertical plume expansion, dilution and entrainment/detrainment due to horizontal plume expansion, lateral diffusion, gas-phase chemistry, surface removal, and surface emission.

The subscript i denotes plume cell i (left or right of the plume centerline), subscript j denotes species j, and superscript t denotes a particular time. Thus, C^t_{ji} is the concentration of species j in cell i at time t, and m^t_{ji} is mass of species j in cell i at time t. In the following derivation of the terms of the mass balance equation for any species j in cell i, the subscript j is omitted for convenience; also, the equations and terms do not show "L" or "R" representing a left or right plume cell, since the equation and terms apply similarly to both sides. Consequently, consider the mass balance of (left or right) cell i (for species j) corresponding to the its expansion during a small time interval dt.

$$\partial m_i = (\partial m_i)_{Disp} + (\partial m_i)_{Emis} + (\partial m_i)_{Chem} + (\partial m_i)_{Dep} \qquad (9\text{-}24)$$

Now, the following expression is also applicable for the plume cell mass.

$$\partial m_i = m_i^{t+dt} - m_i^{t} = C_i^{t+dt} l H_p^{t+dt} W_p^{t+dt} - C_i^{t} l H_p^{t} W_p^{t} \qquad (9\text{-}25)$$

Herein the alongwind dimension in the downwind direction (l = Udt) is prescribed, which is determined from the initial mean transport speed (U) over the time interval dt.

Mathematical expressions are presented in subsequent sections for the updated concentration of species j in cell i due to the action of the individual processes during time interval dt. In the current version of PinG, only surface emissions after plume touchdown are included in the emission term since (non-MEPSE) point-source emissions into grid cells (above the lowest cell layer) neighboring the MEPSE plume are released uniformly into the entire emission grid cell and impact the MEPSE plume only through the boundary conditions. Surface removal is due to dry deposition at the ground. Gas-phase chemistry is included with the full chemical mechanisms of the CCTM in the chemistry term. In the future, the PinG will be adapted to employ the same aerosol module used by the CCTM. No wet processes are treated in the initial PinG version. The current approach to address limitations in the initial version of PinG is to transfer the plume over to the grid solution whenever conditions exist (e.g., precipitation) which the PinG treatment cannot adequately accommodate. This issue will be addressed in more detail in the section on plume handover.

9.3.2.3 Treatment of Plume Expansion and Diffusion Processes

Dispersion affects the mass balance of a plume cell as a result of dilution and entrainment/detrainment processes related to the lateral and vertical expansion of a plume cross-section during a time interval dt, as well as mass diffusion which impacts cell concentrations as a result of concentration gradients between adjacent cells. The dispersion processes can be expressed by

$$(\partial m_i)_{Disp} = (\partial m_i)_{Dil/E/D} + (\partial m_i)_{Dif} \quad (9\text{-}26)$$

where the first term on the right side of Equation 9-26 represents the dilution / entrainment / detrainment processes and the last term is the eddy diffusion process.

The relationships developed herein apply to cells on either side of the plume centerline, since the only difference occurs in their application when different boundary conditions occur at each edge.

$$(\partial m_i)_{Dil/E/D} = (m_i^{t+dt} - m_i^t)_{Dil/E/D} \quad (9\text{-}27)$$

refers to the change of mass in plume cell i (for any transported species j) during dt as a result of dilution and entrainment/detrainment. The changes due to just the horizontal and vertical exchange processes can be expressed by

$$m_i^{t+dt} = m_i^t + (\partial m_i)_{Latdil/E/D} + (\partial m_i)_{Vertdil/E/D} \quad (9\text{-}28)$$

where Latdil refers to horizontal (lateral) dilution. In practice, the lateral dilution/ entrainment/detrainment term in Equation 9-28 is determined and then the last term is solved.

The lateral dilution term in Equation 9-28 is given by

$$(\partial m_i)_{Latdil/E/D} = lH_p^t(C_{i+1}^t \partial y_{i+1} - C_i^t \partial y_i) \quad (9\text{-}29)$$

However, the following relationship also exists.

$$\partial y_i = \eta_i \partial W_p \quad (9\text{-}30)$$

since η is invariant. Therefore, Equation 9-29 can be revised to the following form.

$$(\partial m_i)_{Latdil/E/D} = lH_p^t(\eta_{i+1}C_{i+1}^t - \eta_i C_i^t)\partial W_p \qquad (9\text{-}31)$$

At this time, (i.e., after lateral dilution/entrainment/detrainment) the width of a plume cell is w_i^{t+dt}. With the cell widths remaining unchanged, plume vertical expansion occurs (i.e., in the up and down direction for an elevated plume, and up only after plume touchdown). Let C_a^{t+dt} and C_b^{t+dt} denote the concentrations of species j above and below plume cell i, respectively, for the elevated plume case. C_a and C_b represent the CCTM grid concentrations at t+dt. Once the plume becomes surface-based, only C_a is relevant. The equation for the vertical dilution term is given by

$$(\partial m_i)_{Vertdil/E/D} = lw_i^{t+dt}(C_a^{t+dt}\partial H_a + C_b^{t+dt}\partial H_b) \qquad (9\text{-}32)$$

where the changes in H_a and H_b denote plume vertical expansion of the upper and lower plume boundaries, respectively. An assumption is made that

$$\partial H_a = \partial H_b = 0.5\partial H_p \qquad (9\text{-}33)$$

for an elevated plume cross-section, and after a plume reaches the surface

$$\begin{aligned} \partial H_a &= \partial H_p \\ \partial H_b &= 0 \end{aligned} \qquad (9\text{-}34)$$

are applicable. Equation 9-32 can be rewritten accordingly as

$$(\partial m_i)_{Vertdil/E/D} = lw_i^{t+dt}C_*^{t+dt}\partial H_p \qquad (9\text{-}35)$$

where

$$\begin{aligned} C_*^{t+dt} &= (C_a + C_b) \qquad (elevated\ plume) \\ C_*^{t+dt} &= C_a^{t+dt} \qquad (surface\text{-}based\ plume) \end{aligned} \qquad (9\text{-}36)$$

for an elevated plume and a plume bottom at the surface, respectively. The combination of Equations 9-31 and 9-35 produces the following form.

$$(\partial m^{i})_{Dil/E/D} = lH_p^{t}\partial W_p(\eta_{i+1}C_{i+1}^{t} - \eta_i C_i^{t}) + l\partial H_p w_i^{t+dt} C_*^{t+dt} \tag{9-37}$$

However, by substituting the next expression,

$$(\partial m_i)_{Dil/E/D} = C_i^{t+dt} lH_p^{t+dt} w_i^{t+dt} - C_i^{t} lH_p^{t} w_i^{t} \tag{9-38}$$

and rearranging, the concentration after the total dilution/entrainment/detrainment step is

$$C_i^{t+dt} = C_i H_p^{t} \frac{w_i^{t}}{H_p^{t+dt}} w_i^{t+dt} + \frac{H_p^{t}}{H_p^{t+dt}} \frac{\partial W_p}{w_i^{t+dt}} (\eta_{i+1}C_{i+1}^{t} - \eta_i C_i^{t}) + \frac{\partial H_p}{H_p^{t+dt}} C_*^{t+dt} \tag{9-39}$$

The first term on the right-side is related to the dilution effect and the next two terms are the lateral and vertical entrainment/detrainment effects, respectively. The subsequent expressions are also applicable.

$$\begin{aligned} w_i^{t} &= y_{i+1}^{t} - y_i^{t} = W_p(\eta_{i+1} - \eta_i) \\ w_i^{t+dt} &= W_p^{t+dt}(\eta_{i+1} - \eta_i) = (\eta_{i+1} - \eta_i)(W_p + \partial W_p) \\ H_p^{t+dt} &= H_p^{t} + \partial H_p \end{aligned} \tag{9-40}$$

By substituting the above expressions into Equation 9-39, and rearranging gives

$$C_i^{t+dt} = C_i^{t} \frac{(H_p W_p)^{t}}{(H_p W_p)^{t+dt}} + \frac{\partial H_p}{H_p^{t+ddt}} C_*^{t+dt} + \frac{H_p^{t}}{H_p^{t+dt}} \frac{\partial W_p}{W_p} \frac{(\eta_{i+1}C_{i+1}^{t} - \eta_i C_i^{t})}{(\eta_{i+1} - \eta_i)} \tag{9-41}$$

However, Equation 9-41 can be simplified and re-written as

$$C_i^{t+dt} = \frac{1}{1+\lambda_H}\left((\lambda_H C_*^{t+dt} + \frac{1}{1+\lambda_W}[(C_i^t + \frac{\lambda_w}{\eta_{i+1} - \eta_i}(\eta_{i+1}C_{i+1}^t - \eta_i C_i^t)] \right) \qquad (9\text{-}42)$$

where

$$\lambda_H = \frac{\partial H_p}{H_p} \quad , \quad \lambda_W = \frac{\partial W_p}{W_p} \quad . \qquad (9\text{-}43)$$

When applying Equation 9-42, certain boundary conditions must be specified. In particular, if

$$\begin{aligned} i &= 1 \quad ; \quad \eta_i = \eta_1 = 0 \\ i &= N_L \, , \, i = N_R \quad ; \quad C_{i+1} = C_{bg}^{t+dt} \end{aligned} \qquad (9\text{-}44)$$

where C_{bg}^{t+dt} and C_*^{t+dt} are the particular grid cell concentrations from the CCTM solution for the current time step.

In the execution of the CCTM/PinG, both the grid-cell and plume-cell concentrations are updated by numerical integration of the corresponding mass balance equations from time t to t+dt, where dt is the CCTM advection time step (MSTEP). The sequence is that CCTM performs this integration and updates the concentration field first, generating C^{t+dt} in each grid cell, before PinG is called to do the same. PinG performs the integration in a fractional step approach; first for plume dispersion (step 1) then for the surface emission and removal processes (step 2), and finally for plume chemistry (step 3). The chemistry integration is actually performed in smaller chemistry time steps, internally determined for the plume cells by the chemical solver, in sequence, until the integration is completed for the time interval dt. The emission/removal step is implemented in a single integration time step. The dispersion step is performed sequentially in subtime steps until dt is reached. The PinG dispersion time step is constrained by a restriction when applying Equation 9-42 arising from the fact that, in a given time step, the location after expansion of the inner interface of a given plume cell (i.e. y_i^{t+dt}) cannot pass beyond the location of the outer interface of that cell at the start of the ex expansion. Therefore, the following constraint applies.

$$y_i^{t+dt} \le y_{i+1}^t \quad , \quad 2 \le i \le N_{L\,,\,R} \qquad (9\text{-}45)$$

This criterion requires that the following limit for the PinG time step must be satisfied.

$$\partial t_{disp} \leq \frac{(\eta_{i+1} - \eta_i)}{\eta_i} \frac{1}{\lambda_W^*} \tag{9-46}$$

$$\lambda_W^* = \frac{1}{W_p} \frac{dW_p}{dt} \tag{9-47}$$

It should also be noted that λ_W^* is related to λ_w according to

$$\lambda_w = \int_t^{t+dt} \lambda_w^* dt \tag{9-48}$$

During the model simulation, W_p (t) and dW_p/dt are provided to the PinG module from the PDM data file. Thus, λ_W^* is determined directly, and λ_W can also be computed using the plume widths from time t and t+dt.

The dispersion step is not complete without inclusion of the diffusion term. The diffusion equation of a species concentration for any plume cell i may be expressed by

$$\frac{\partial C_i}{\partial t} = \frac{\partial}{\partial y}(K_y \frac{\partial C_i}{\partial y}) \tag{9-49}$$

where K_y is the horizontal eddy diffusion coefficient. It can be expressed by

$$K_y = \frac{1}{2} \frac{d}{dt}(\sigma_y^2) \tag{9-50}$$

By applying the relationship between σ_y and W_p in Equation 9-1, the following form for K_y can be derived.

$$K_y = \frac{W_p^2}{a^2} \lambda_w^* \tag{9-51}$$

Numerical integration of a form like Equation 9-49 is solved with the Crank-Nicholson method in which centered differencing is used for both time and space derivatives to solve the diffusion equation. This technique provided stable numerical solutions compared to an explicit method. The resulting finite-difference equation is then solved by matrix decomposition of the coefficient-matrix into upper and lower (LU) triangular matrices. For convenience in setting up the matrix form of the finite difference diffusion equation for all plume cross-section cells, a set of simultaneous equations is developed which are written in a vector-matrix form for solving by LU decomposition.

The derivation of the set of equations is provided. By averaging Equation 9-49 in time to obtain $\partial C/\partial t$ at $t+\partial t$, and using center-differencing to solve for $\partial^2 C/\partial y^2$, simplification leads to

$$C_{i-1}^{k+1}\left[-\frac{K_y\partial t}{(y_{i+1}-y_i)(y_{i+1}-y_{i-1})}\right] + C_i^{k+1}\left[1+\frac{K_y\partial t}{(y_{i+1}-y_i)(y_{i+2}-y_i)}\right] + \frac{K_y\partial t}{(y_{i+1}-y_i)(y_{i+1}-y_{i-1})}\Bigg]$$
$$+ C_{i+1}^{k+1}\left[-\frac{K_y\partial t}{(y_{i+1}-y_i)(y_{i+2}-y_i)}\right] = C_{i-1}^{k}\frac{K_y\partial t}{(y_{i+1}-y_i)(y_{i+1}-y_{i-1})}\Bigg]$$

$$+ C_i^k\left[1 - \frac{K_y\partial t}{(y_{i+1}-y_i)(y_{i+2}-y_i)} - \frac{K_y\partial t}{y_{i+1}-y_i)(y_{i+1}-y_{i-1})}\right] + C_{i+1}^k\left[\frac{K_y\partial t}{(y_{i+1}-y_i)(y_{i+2}-y_i)}\right] \quad (9\text{-}52)$$

where small k is used as a time index for time t, and k+1 represents $t+\partial t$, i is the index to the left edge of plume cell i, and y is the distance from the new reference position at the left background location of the plume cross-section. By using the relationship that $y_i = \eta_i W_p$, the following relations can be defined.

$$\alpha_i = \frac{K_y\partial t}{W_p^2}\frac{1}{(\eta_{i+1}-\eta_i)(\eta_{i+1}-\eta_{i-1})} \quad (9\text{-}53)$$

$$\gamma_i = \frac{K\partial t}{W_p^2}\frac{1}{(\eta_{i+1}-\eta_i)(\eta_{i+2}-\eta_i)} \quad (9\text{-}54)$$

$$\beta_i = \alpha_i + \gamma_i \tag{9-55}$$

By substituting the above expressions into Equation 9-52, the following formula is obtained.

$$-\alpha_i C_{i-1}^{k+1} + (1+\beta_i) C_i^{k+1} - \gamma_i C_{i+1}^{k+1} = \alpha_i C_{i-1}^{k} + (i-\beta_i) C_i^{k} + \gamma_i C_{i+1}^{k} \tag{9-56}$$

Equation 9-56 represents a system of simultaneous equations in the form,

$$Ax = b \tag{9-57}$$

where, $x = (C_i^{k+1} + ...C_{N+2}^{k+1})^t$ and N is the total number of plume cells. Additionally, the expression, A = I - G, is defined where A is a square matrix of size (N+1)x(N+2), and $b = (I+G)C^k$. In these expressions, I is the identity matrix, and G is a tridiagonal matrix of the form, G = tridiag (α, β, γ) , and is of size (N+2)x(N+2). Subsequently, the simultaneous system of equations given by Equation 9-57 is solved using LU decomposition.

The boundary conditions are also included in the above system of equations since N+2 is used. Appropriate boundary conditions are provided by the CCTM grid concentrations for the right and left edges of each plume cross-section. At left edge boundary, $\alpha_1 = \beta_1 = \gamma_1$ and $b_1 = C_1 = C_{bg}^{L}$. At the right edge boundary, α_{N+2} , β_{N+2}, and γ_{N+2} are zero which leads to $b_{n+2} = C_{N+2} = C_{bg}^{R}$.

9.3.2.4 Surface Area Emissions and Dry Deposition

During the PinG simulation, surface emissions are injected into individual surface-based plume cells. The surface emissions, contained in layer 1 values of the 3-D emissions file which is also employed by the CCTM, are used in all plume cells of a plume cross-section. For each grid cell, there is an emission rate for certain species (q_j). In particular, a MEPSE plume cross-section passes over such gridded surface emissions. Consequently, the change in concentration of plume cell i during a time step from surface emissions is

$$\partial C_i^j = k_j \frac{q_j}{\Delta x \Delta y} \frac{\partial t}{H_p} \tag{9-58}$$

where k_j herein is an appropriate species-specific factor for the conversion of concentration from a mass unit to the appropriate volume unit.

Since the PinG formulation is composed of a single vertical layer, it was not designed to have the capability to properly ingest other elevated point-source emissions into the MEPSE plume cross-section. As long as such an along-path, point-source emission remain at a relatively low value, the impact on the MEPSE concentration field is assumed to be felt through background entrainment of the expanding MEPSE plume. If the other point source emission was ingested, of course, such entrained mass is currently dispersed instantaneously throughout the vertical extent of the plume. For this reason, when point-source emissions larger than a critical value are encountered by the MEPSE plume, the current logic is to handover the MEPSE plume to the grid solution.

Dry deposition is a sink term and occurs at the bottom of each plume cell based on the deposition velocity concept.

$$\frac{\partial C_i^j}{\partial t} = - \frac{V_d^j}{H_p} C_i^j \qquad (9\text{-}59)$$

where C_i^j denotes the concentration of species j and the species-specific deposition velocity (V_d^j) values are available from a gridded data file. The same deposition velocity is applied to all cells of a plume section using the V_d values from the grid cell in which the plume centerline is located.

9.3.2.5 Gas-phase Chemistry of Plumes

A gas-phase chemistry mechanism implemented in the CCTM is also invoked by the PinG module. The current mechanisms include the RADM2 and carbon bond (CB-4) chemical mechanisms. Details about these chemical mechanisms are provided in section 8. In addition, there is a separate PinG module version for each chemical solver (i.e., SMVGEAR and QSSA). Minor revisions were needed in the PinG versions of the solver codes to customize them to deal with the plume concentration array whose dimensionality differs from the CCTM gridded concentration array. Nevertheless, the PinG gas photochemistry treatment is identical to that of the CCTM. Since only gas-phase plume chemistry has currently been implemented, when conditions conducive to extensive aqueous chemistry are encountered, a plume section is transferred to the CCTM grid system, as discussed in the handover section below. Future plans include implementation of the existing CCTM aerosol module into PinG so that it also has the capability to treat aerosol and particulate species.

9.3.2.6 Plume Initialization

The initialization of each plume cross-section is the first key procedure performed at the start of its simulation. The PinG initialization of a new MEPSE release occurs when a plume cross-section width reaches a minimum width. The width criterion is a user-specified variable and it is specified for the PDM simulation. A flag indicator variable in the PDM file communicates to PinG when a plume cross-section is ready to be initialized. The current minimum width for initialization of a MEPSE plume section has tentatively been set at 2 km. At initialization, it is

assumed that the lateral concentration distribution across the plume section of the primary emission species exhibits a Gaussian shape. For all other species, initial concentrations have been set to a machine minimum-value (ie. 10^{-30}).

The lateral concentration distribution of the primary species in the plume cells (i.e., "initial condition" of the plume concentration field) is given by

$$C_{ij}(0) = k_j \frac{q_j}{UH_p} \frac{1}{2\pi\sigma_y} \exp[-0.5(y_i^*/\sigma_y)^2] \qquad (9\text{-}60)$$

where, y^* is $(y_i - y_o)$, the distance of the outer edge of cell i from the plume centerline, and U is the mean transport speed, q_j is the MEPSE emission rate of species j, and k_j is the appropriate species specific mass-to-volume conversion factor.

In PinG, it is assumed that the MEPSE emissions are at an hourly resolution, and that we are performing plume simulations of hourly releases. The assumption is made that the emission rate (q_j) remains constant over the hour. Consequently, at the handover time, the transformed mass impacted by the various plume dynamic and chemical processes corresponding to one hour of emission is released to the grid solution.

9.3.2.7 Methodology for Plume Feedback to the Eulerian Grid

When the subgrid scale phase of a plume section simulation has been completed, the plume material is ready for transfer to the CCTM grid. The total concentration of each species in any plume cell is composed of a component equal to the background concentration, and an additional component consisting of the plume concentration, which differs from the background grid level. In performing the handover, the conceptual basis is that only the plume component is related to the corresponding MEPSE emissions. Thus, the feedback is restricted to the plume contribution. Additionally, since hourly plume releases are simulated from each MEPSE source in PinG, and since the assumption has been made that each such hourly emission remains constant for the full hour, the current practice is to handover the contents of a plume section corresponding to a full hour release. Thus, for each plume species,

$$m_P = V_p(\overline{C_p} - \overline{C_{bg}}) \qquad (9\text{-}61)$$

where average values for the plume and background grid concentrations are employed. The average plume concentration (C_p) of each species is determined from all plume cells. The background grid value (C_{bg}) represents the average of the CCTM grid-cell concentrations on each side of the plume for all appropriate layers over the vertical extent of the plume. The handover plume mass is distributed into the column of cells up to H_p in which the plume

centerline is located at the handover time. The feedback of plume mass represents an adjustment to the CCTM grid cell concentrations from an average concentration (C_{adj}). From a mass balance perspective,

$$\overline{C_{adj}}V_G = (\overline{C_p} - \overline{C_{bg}})V_p \quad (9\text{-}62)$$

where V_G is the CCTM grid cell volume. The plume volume (V_p) is determined from

$$V_p = W_p H_p (U\Delta t) \quad (9\text{-}63)$$

where U is the mean horizontal wind speed, Δt is a 1-hour interval and $U\Delta t$ corresponds to the alongwind dimension (Δx_p) spanned by the plume section. In a similar fashion, the grid volume impacted by the plume is given by

$$V_G = \Delta x_G \Delta y_G (Z_G^t - Z_G^b) \quad (9\text{-}64)$$

where Δx_G and Δy_G are the horizontal grid cell sizes, and Z_G^t and Z_G^b are the heights of the top and bottom of the model layers spanned by the plume.

Substituting the above expression into Equation 9-62 yields:

$$\overline{\overline{C_{adj}}} = (\overline{\overline{C_p}} - \overline{\overline{C_{bg}}})\frac{H_p W_p \Delta x_p}{V_G} \quad (9\text{-}65)$$

In the initial release version of PinG when plume handover is triggered, an entire hour's worth of plume release in its transformed state is transferred to the appropriate column of grid cells during a CCTM advection time step. In the future, the intention is to incrementally transfer the same plume excess to the impacted grid cells over a one hour period of model time steps. In this manner, the continuous emissions after being treated in PinG would be transferred during a one hour period following the handover time.

PinG simulations are primarily intended for the coarse-grid, regional modeling grid sizes with the horizontal resolution (Δ) of nominally 20-40 km. Daytime MEPSE plumes reach or are close to chemical maturity when the plume width attains these grid sizes. However, PinG simulations at finer grid sizes are possible, however, test runs have not been performed but are needed in order to assess the benefits of this approach at urban grid cell sizes. As the primary purpose of PinG is

to improve the subgrid-scale treatment of large point-source plumes, the key handover size criterion based on plume width relative to grid cell size has been prescribed according to

$$\frac{W_p}{\Delta} \geq \gamma_{cr} \qquad (9\text{-}66)$$

The default value for γ_{cr} is 1.0. Therefore, when a plume section width attains the grid cell size, a flag indicator variable generated by PDM triggers PinG to perform the handover process. Currently, the CCTM system is operated in a 1-way nesting mode, as multiple nested grids are not performed in a single simulation. Consequently, PinG is not equipped to handle the movement of a plume from a larger to a finer gridded domain within the same simulation.

Ideally, plume handover also occurs when the plume has also reached chemical maturation when concentration differences within the plume become rather small. A chemical criterion also incorporated into PinG involves a default condition recognizing chemical maturation. It is based on an average plume concentration ratio of O_3/O_x ,where $O_x = O_3+NO_2$ denotes the principal oxidant species using concentrations from all cells in a plume section. This ratio is employed as a surrogate indicator of plume chemical age. The specific chemical maturation criterion is:

$$\frac{\overline{O_3}}{\overline{O_x}} \geq r_{chem} \qquad (9\text{-}67)$$

where r_{chem} represents the critical value. The default value has been set at 0.99. Tests have indicated this value to be a good indicator corresponding to a chemically-mature stage 3 plume.

The use of O_3 / O_x as a surrogate for plume age is not common compared to NO_x / NO_y where NO_y includes all the reactive oxides of nitrogen. However, NO_x/NO_y has not been applied as a chemical criterion because injection of fresh emissions from large point sources has been observed to suddenly decrease the chemical age of the background which leads to "premature" activation of the chemical criterion. Experience from testing with the first chemical criterion has proved it to be more satisfactory.

In the initial version of the Models-3 PinG , additional criteria are needed which can also trigger plume handover to the Eulerian grid cells. As the PinG module is upgraded in the future, the these criteria may be avoided.

The next two criteria are related to non-MEPSE emissions in the immediate vicinity of a MEPSE plume cross-section.

Urban Criterion

PinG currently does not have the facility to injest different surface emissions into individual plume cells. Such a condition is likely to be encountered by a MEPSE plume after touch-down when it passes over an urban-industrial area with a very inhomogeneous spatial distribution of emissions. Gillani and Pleim (1996) have identified such "urban" areas based on the following criterion pertaining to the emissions of NO_x .

$$f_q\ (NO_x) \succ 10^{12} \quad molecules/cm^2/s \tag{9-68}$$

This condition denotes a fairly high NO_x surface emission flux (f_q). The critical value of 10^{12} chosen by Gillani and Pleim (1996) was based on an emission inventory with a horizontal spatial resolution of about 20 km. For such a grid size, this condition corresponds to an emission rate of about 0.3 kg/s. Thus, the selected "urban" emissions handover criterion is:

$$q_{NOx} \succeq 0.3 \quad kg/s \tag{9-69}$$

The above condition must be satisfied to trigger plume section handover, and the plume bottom must also be at the ground for this criterion to activate.

Point-source Emissions Criterion

The initial PinG version does not possess multiple vertical layer resolution of the plume. Thus, if a plume section entrains the elevated concentration of a primary species in a background grid cell from a fresh NO_x emission from a non-MEPSE major point source, such entrained mass is instantaneously mixed vertically throughout the MEPSE plume. If the non-MEPSE point source emission is large enough, the related error of its treatment in the MEPSE plume relative to its treatment in the gridded solution becomes large. Thus, it is advantageous to handover the MEPSE plume under this circumstance. A handover criterion of 3.33×10^{-6} ppm/s has been set which corresponds to about 2 ppb/10 minutes. If the new non-MEPSE point-source emissions in the immediate vicinity of the MEPSE plume are large enough to raise the average background concentration (left/right and vertically-averaged over MEPSE plume height) by more than 2 ppb in 10 minutes, then handover is also triggered.

Precipitation Criterion

PinG has no facility to handle wet removal of the plume. Consequently, if the total (convective and non-convective) precipitation rate in the cell containing the MEPSE centroid exceeds a

critical value, a plume handover is also triggered. Currently, the default value of this critical precipitation rate is 0.00008 cm/s or about 0.3 cm/hr.

Excessive Wind-Shear Criterion

Since the plume treatment is PinG is based on a Lagrangian simulation for a single vertical layer, there is no facility to properly treat the effect of wind shear. When excessive speed wind shear over the vertical extent of the plume exceeds a critical value, plume section handover will occur on the basis that the treatment of such wind shear will be better treated in the multi-layer grid model.

Domain Boundary Criterion

Finally, a MEPSE plume section is transferred to grid cell in which the centroid of the MEPSE is located if it is about to exit the gridded domain. Otherwise the plume concentration contribution cannot be accounted for if the plume travels beyond the model domain boundary.

In all handover cases considered above, the entire MEPSE plume section is transferred. There is a particular condition in which only a top portion of the plume may be handed over, while the remaining part of the plume continues to be simulated. This type of premature partial handover is forced because PinG does not possess adequate vertical resolution, and also because the plume simulation in PinG is based on a Lagrangian approach. This condition arises when the plume is well-mixed throughout the daytime PBL, and the PBL height decreases significantly along the path of the plume, for whatever reason. In reality, in such a case, the plume would be split between an upper portion above the PBL and a lower portion remaining within the PBL. The two portions could then experience very diverse stability and flow conditions which cannot be accommodated in the current version of PinG.

The approach is that once the PBL height begins to decrease, and it decreases by more than 15% of the previous z_i , the plume section is handed over. However, the lower portion continues to be simulated. If the decrease in z_i is temporary and it later begins to increase again, the remaining simulated plume would expand vertically just as if it was the full plume. When z_i continues to decrease, as during the evening transition period, then the partial handover would continue incrementally as the PBL decreases by each 15% segment until the nocturnal mixing height is reached, at which time the remaining plume is also handed over. In this manner, PinG does not continue to simulate the well-mixed daytime plume into the night. This approach avoids the Lagrangian simulation of the deep night-time plume which frequently experiences substantial wind shear conditions related to nocturnal jets and inertial oscillations.

The situation is different for a fresh MEPSE release into the nocturnal stable layer above the shallow mixing layer. Such a plume is likely to be thin in the vertical and, therefore, not very likely experience excessive shearing conditions. In our Lagrangian approach, therefore, PinG will generally simulate fresh nighttime plume sections which do not experience excessive shear because of their limited vertical extent.

9.3.2.8 Test Application of the Plume-in-Grid Modeling Approach

The schematic diagram in Figure 9-8 shows how the PDM and PinG fit into the overall Models-3 CMAQ system of science programs. Since PDM serves as a processor program, it is exercised in advance of the CCTM/PinG simulation. PDM requires the MEPSE stack parameter file generated by the MEPPS emissions system, and a set of meteorological data files prepared by MCIP from an MM5 simulation. The details of these input files which are needed to perform a PDM simulation are described in the Models-3 user guide (EPA, 1998). Input and output parameters for the PDM processor are also defined in the user guide.

The PinG module is an integral part of the CCTM, as depicted in Figure 9-8, and it is invoked by the CCTM driver program along with the other science processes. In the sequence of processes, PinG is called just before the grid model performs the gas-chemistry step. Consequently, when PinG completes a time step, the CCTM driver calls the chemistry to undertake gas-photochemistry on the 3-D gridded array. When PinG is being exercised, it needs data files generated by ECIP, MCIP, PDM and also the MEPSE emission file from MEPPS processing. The PinG module also generates a plume concentration file containing the species concentrations in each plume cell for each plume cross-section. Since the PinG concentration file is a Models-3 specific format, it can be viewed in a visualization software package designed for such data files. In addition, an effort is planned to visualize both the plume and grid concentrations on the same display.

The plume-in-grid algorithms were exercised for a single MEPSE within a 36 km gridded domain. The plume cell O_3 concentrations in Figure 9-9 are for various times from a selected plume section released during the early afternoon. The PinG module simulated 10 plume cells in this plume section, with the concentrations on each edge of the cross-section at various times being the CCTM gridded values used as background conditions. It is evident that the modeled O_3 concentrations displays the same chemical stages described earlier. A significant ozone deficit exists in the narrow plume for 1-2 hours after release. As the plume expanded, the O_3 concentration gradually recovers and exhibits higher O_3 in some cells outside the plume core of the cross-section at 15:30 than the grid value at each edge or in the plume core. This represents stage 2 of plume chemical evolution. Eventually, stage 3 was attained as all plume cell O_3 concentrations exceeded the CCTM concentrations on each side of the plume with the maximum excess of about 10 ppb in this case. Shortly after 1730 LST, the last time displayed in Figure 9-9 for this plume section, it was transferred to the CCTM grid system. Therefore, this plume section was active in the subgrid phase about 5 hours in this case. Once the feedbeack of a plume section occurs, PinG no longer simulates it which reduces computational time.

The results of this test case and others not described herein are encouraging since they compare rather favorably in a qualitative sense with observed concentrations (not shown) across the same MEPSE plume at about the same time. Nevertheless, an extensive evaluation of the PinG is planned for several case study days with plume data for various species obtained during the Southern Oxidant Study 1995 experimental intensive program conducted in the Nashville,

Tennessee area. The evaluation will assess the capability of the PinG components to treat pollutant plumes and determine the impacts on the regional grid concentrations.

9.4 Summary

A plume-in-grid technique has been developed for use in the Models-3 Community Multiscale Air Quality modeling system. The key algorithms include a plume dynamics Model (PDM) processor designed to generate a data file for use in the PinG module simulation. The PinG module has been fully integrated into the CCTM Eulerian grid model to provide a more refined, realistic treatment of the physical and chemical processes impacting selected major point source emissions during a subgrid scale plume phase in a regional model application. The initial release version is limited to performing gas-phase photochemistry within the plumes. A future PinG version is expected to include an aerosol and particulate modeling capability. Test simulation results have been conducted and qualitative results are encouraging regarding the treatment of plume growth and plume concentrations. However, a rigorous diagnostic evaluation of the various processes is planned using the 1995 Southern Oxidant Study-Nashville experimental plume data. Future advancements and refinements of the initial plume-in-grid algorithms are anticipated and upgraded algorithms will be reflected in upcoming releases.

9.5 References

Arya, P., 1984: Parametric relations for the atmospheric boundary layer. Boundary-Layer Meteorol.,30, 57-73.

Briggs, G.A., 1975: Plume rise predictions. In: Lectures on Air Pollution and Environmental Impact Analyses, Workshop Proceeding, Boston, MA, 1975, pp 59-111.

Chang, J.S., K.H. Chang, and S. Jin, 1993: Two-way and one-way nested SARMAP air quality model. International Conf. on Regional Photochemical Measurement & Modeling Studies, November 8-12, San Diego, CA, A&WMA, Pittsburgh, PA.

Clarke, J.F., J. Ching, J.M. Godowitch, 1983: Lagrangian and eulerian time scales relationships and plume dipsersion from the Tennessee Plume Study. Sixth Symp. on Turbulence and Diffusion, March 22-25, 1983, Amer. Meteorol. Soc., Boston, MA.

Draxler, R.R, 1976: Determination of atmospheric diffusion parameters. Atmos. Environ., 10, 99-105.

EPA, 1998: Models-3 Volume 9b: User Manual, EPA-600/R-98/069b, U.S. Environmental Protection Agency, Research Triangle Park, NC 27711.

Gillani, N.V. and W.E. Wilson, 1980: Formation and transport of ozone and aerosols in power plant plumes. Ann. N.Y. Acad. Sci., 338, 276-296.

Gillani, N.V., S. Kohli, and W.E. Wilson, 1981: Gas-to-particle conversion of sulfur in power plant plumes: I: Parameterization of the conversion rate for moderately polluted ambient conditions. Atmos. Environ., 15, 2293-2313.

Gillani, N.V. and J. E. Pleim, 1996: Subgrid scale features of anthropogenic emissions of NOx and VOC in the context of regional eulerian models. Atmos. Environ., 30, 2043-2059.

Gillani, N.V., 1986: Ozone Formation in pollutant plumes: A reactive plume model with arbitrary crosswind resolution. U.S. Environmental Protection Agency, EPA-600/3-86-051, Research Triangle Park, NC, 85 pp.

Gillani, N.V., 1996: Personal communication.

Godowitch, J.M., J. Ching, and N.V. Gillani, 1995: A treatment for Lagrangian transport and diffusion of subgrid scale plumes in an eulerian grid framework. Eleventh Symp. on Boundary Layers & Turb., March 27-31, Charlotte, NC, Amer. Meteorol. Soc., Boston, MA, 86-89.

Hanna, S.R., G.A. Briggs, and R.P. Hosker, 1982: Handbook on atmospheric diffusion, U.S. DOE, DOE/TIC-11223, DE82002045, National Technical Info. Center, Springfield, VA.

Hanna, S.R., 1984: Applications in air pollution modeling, Chap. 7, Atmos. Turb. & Air Poll. Modeling, Ed. F.T.M. Nieuwstadt and H. van Dop, D. Reidel Publishing Co., Kluwer Academic Publishers, Hingham, MA.

Hicks, B.B., 1985: Behavior of turbulence statistics in the convective boundary layer. J. of Clim. and Applied Meteorology. 24, 607-614.

Irwin, J.S., 1979: Scheme for estimating dispersion parameters as a function of release height, EPA-600/4-79-062, Research Triangle Park, NC., 56 pp.

Irwin, J.S., 1983: Estimating plume dispersion - a comparison of several sigma schemes. J. Clim. And Appl. Meteorol., 22, 92-114.

Kumar, N. and A.G. Russell, 1996: Development of a computationally efficient, reactive sub-grid scale plume model and the impact in the northeastern United State using increasing levels of chemical detail. J. of Geophys. Res., 101, 16737-16744.

Mathur, R., L.K. Peters, and R.D. Saylor, 1992: Sub-grid presentation of emission source clusters in regional air quality modeling. Atmos. Environ., 26A, 3219-3238.

Morris, R.E. M.A. Yocke, T.C. Myers, and V. Mirabella, 1992: Overview of the variable-grid Urban Airshed Model (UAM-V) 85th Annual Meeting of the A&WMA, June 21-26, 1992, Kansas City, MO., AWMA, Pittsburgh, PA.

Myer, T.C., P.D. Guthrie and S.Y. Wu, 1996: The implementation of a plume-in-grid module in the SARMAP air quality model (SAQM). SYSAPP-96-06, Systems Applications International, Inc., Available from Technical Support Div., California Air Resources Board, Sacramento CA.

Niewstadt, F.T.M., 1984: Some aspects of the turbulent stable boundary layer. Boundary-Layer Meteorol., 30, 31-55.

Odman, M. T. and A.G. Russell, 1991: Multiscale modeling of pollutant transport and chemistry. J. of Geophys. Res., 96, D4, 7363-7370.

Pasquill, F., 1976: Atmospheric dispersion parameters in Gaussian plum modeling: Part II. Possible requirements for change in the Turner workbook values. EPA-600/4-76-030b, US EPA, Research Triangle Park, NC , 53 pp.

Pasquill, F., 1979: Atmospheric dispersion modeling. J. of the Air Poll. Contrl. Assoc., 29, 117-119.

Seigneur, C., T.W. Tesche, P.M. Roth, and M.K. Liu, 1983: On the treatment of point source emissions in urban air quality. Atmos. Environ., 17(9), 1655-1676.

Turner, D.B., T. Chico and J.A. Catalano, 1986: TUPOS - a multiple source gaussian dispersion algorithm using on-site turbulence data. U.S. Environmental Protection Agency, EPA/600/8-86-010, National Technical Information Center, Springfield, VA.

Venkatram, A., D. Strimaitis, D. Cicristofaro, 1984: A semiempirical model to estimate dispersion of evelated releases in the stable boundary layer. Atmos. Environ., 18, 923-928.

Venkatram, A. 1988: Dispersion in the stable boundary layer. Chapter 5, In Lectures on Air Pollution Modeling, A. Venkatram abd J. Wyngaard, Eds., Amer. Meteorol. Soc., Boston, MA., 1988.

Weil, J.C., 1988: Dispersion in the convective boundary layer. Chapter 4, In Lectures on Air Pollution Modeling, A. Venkatram and J. Wyngaard, Eds., Amer. Meteorol. Soc., Boston, MA., 1988.

This chapter is taken from *Science Algorithms of the EPA Models-3 Community Multiscale Air Quality (CMAQ) Modeling System*, edited by D. W. Byun and J. K. S. Ching, 1999.

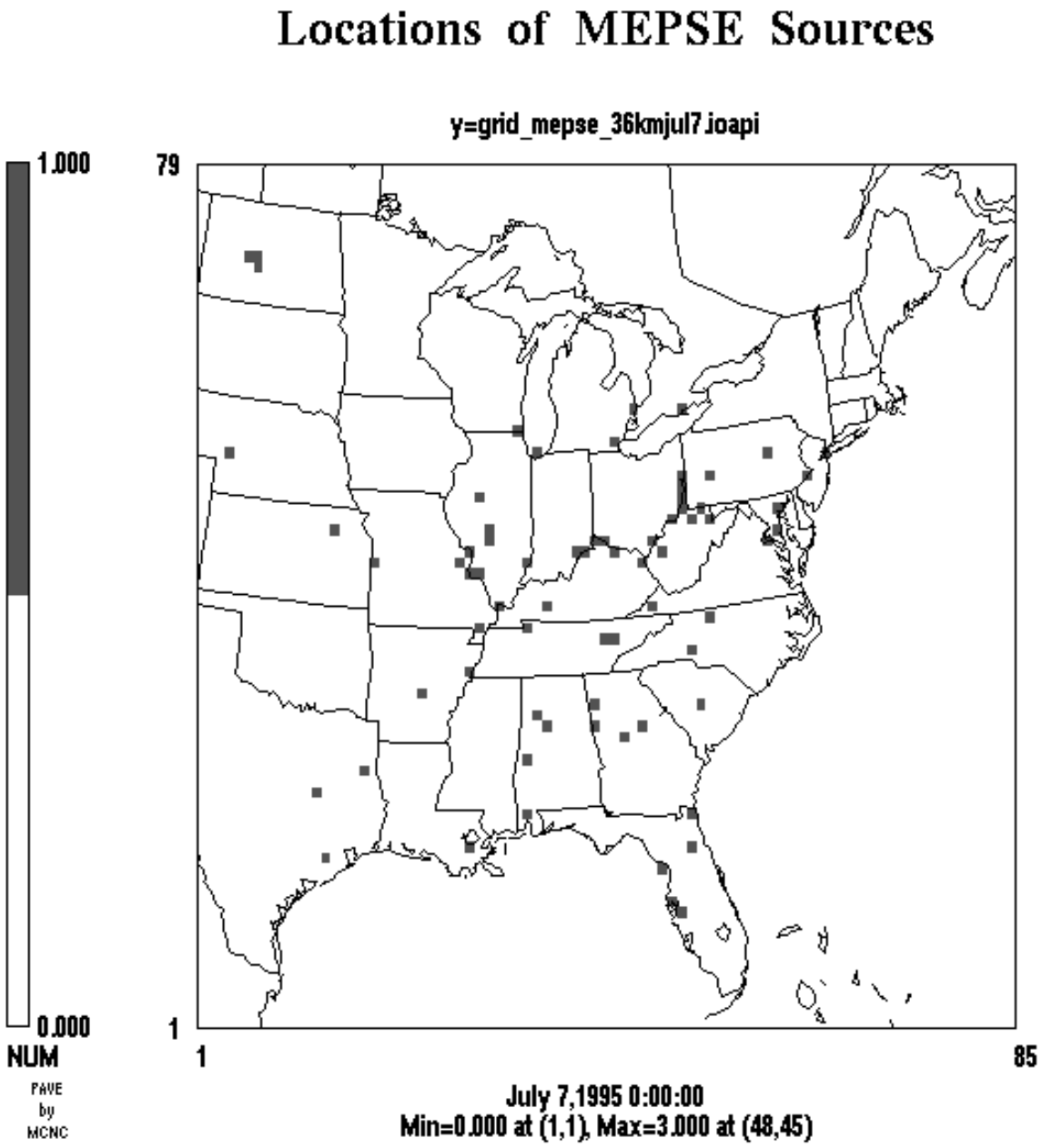

Figure 9-1 Location of MEPSEs depicted in individual grid cells.

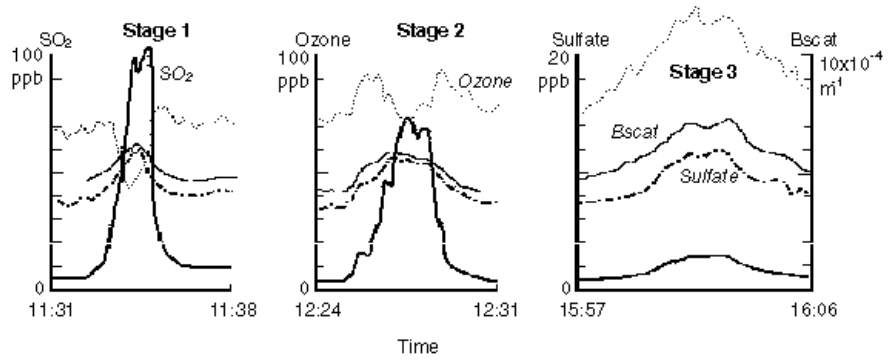

Figure 9-2. Chemical stages of a plume are depicted by aircraft plume data of SO2, ozone, sulfate, and aerosol scattering coefficient (Bscat) from crosswind traverses through a large MEPSE plume. Measurements are from the daytime period of the 23 August 1978 Tennessee Plume Study experiment. (Adapted from Gillani et al, 1981)

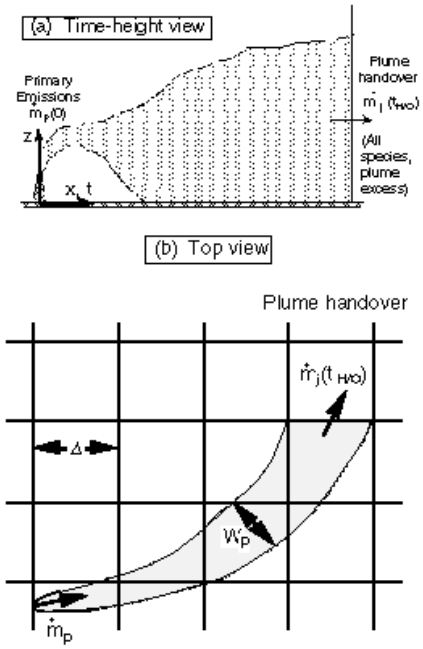

Figure 9-3. Schematics of the a) time-height view and b) top view of the modeling concept of the subgrid scale plume in the Models-3 PinG approach.

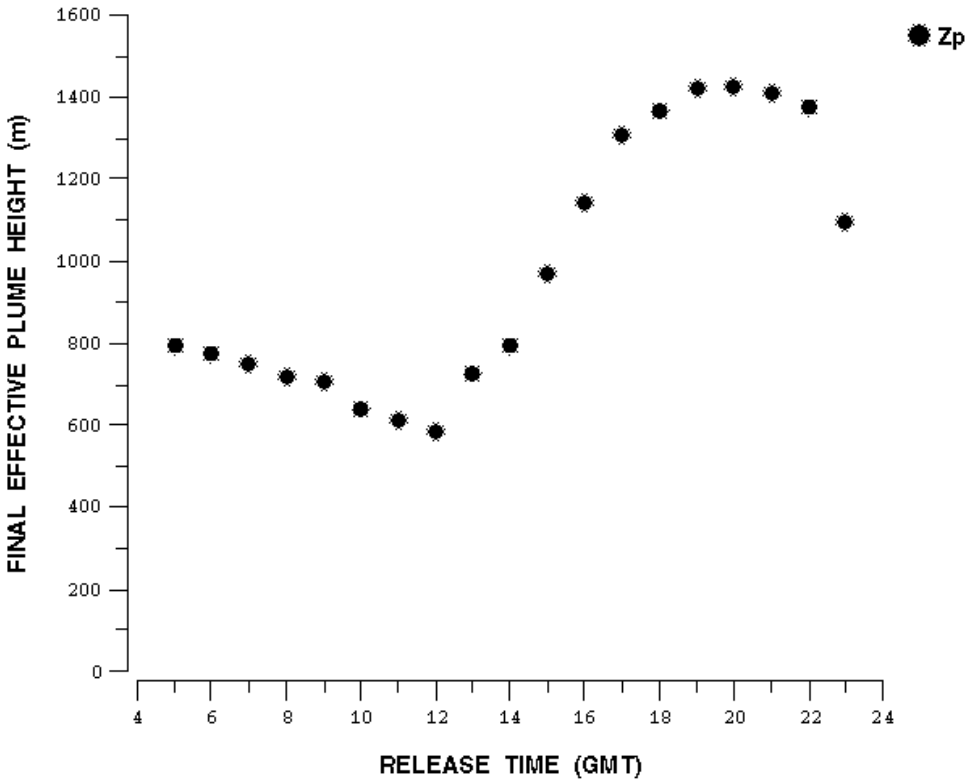

Figure 9-4. Example of the final plume height after plume rise for hourly releases from a MEPSE 300 m stack height.

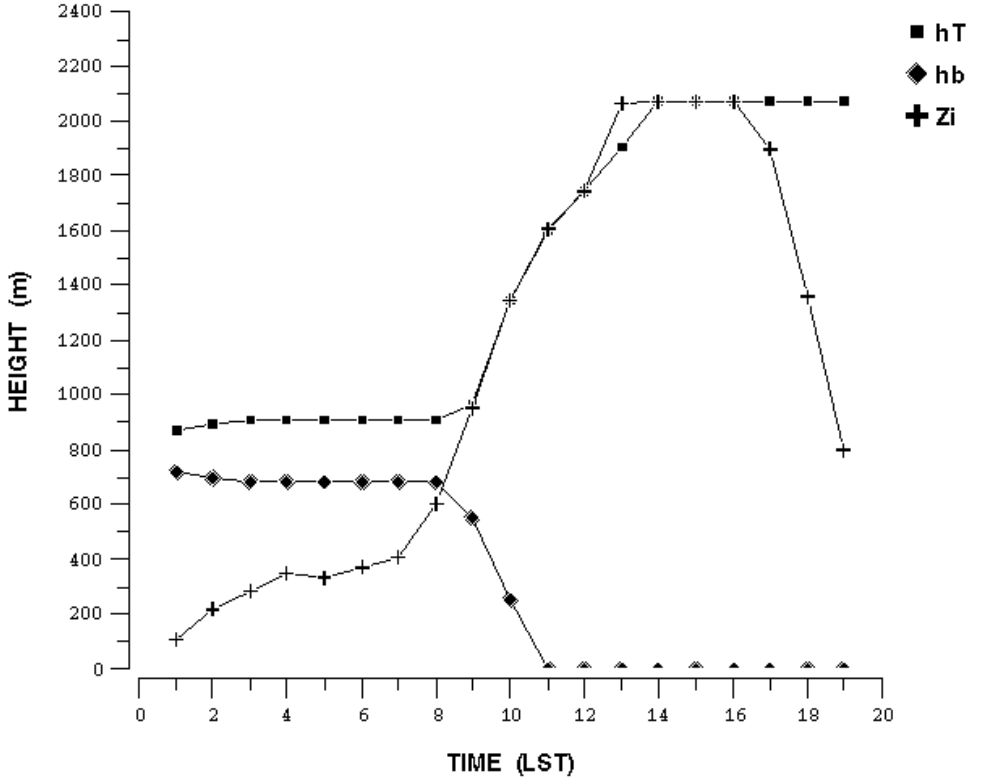

Figure 9-5. Time variation of the plume bottom (hb) and top (hT) heights and the PBL height (Zi) for a nocturnal release.

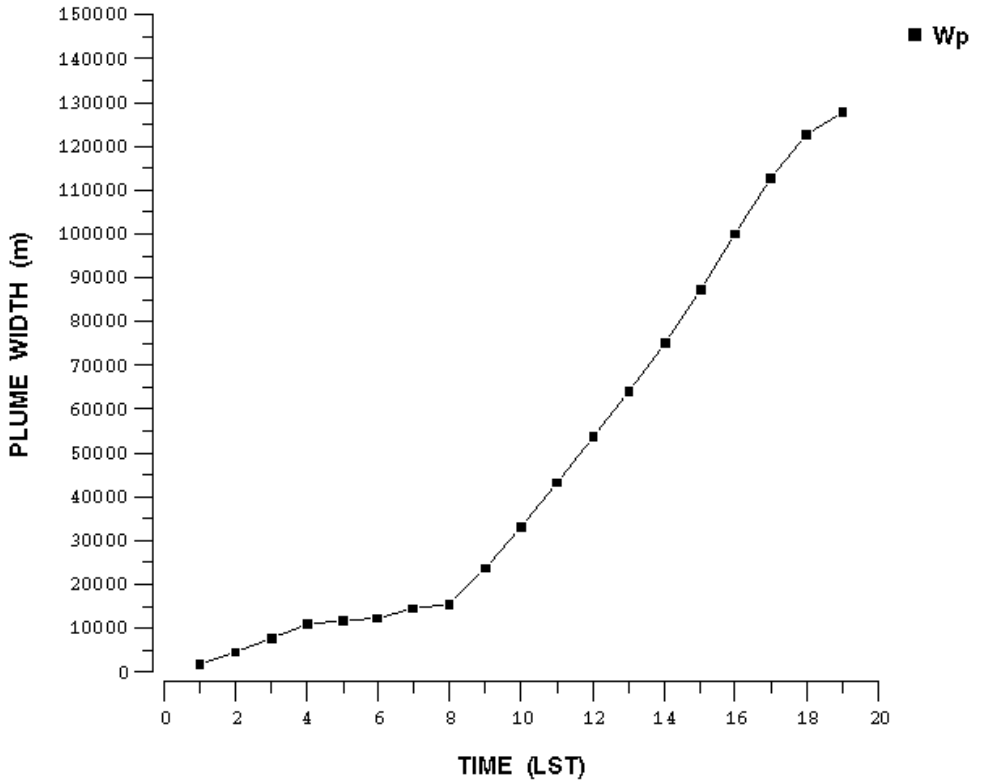

Figure 9-6. Time variation of plume width (Wp) from a nocturnal plume release. A plume width of about 30 km is achieved during the morning period about 10 hours after release.

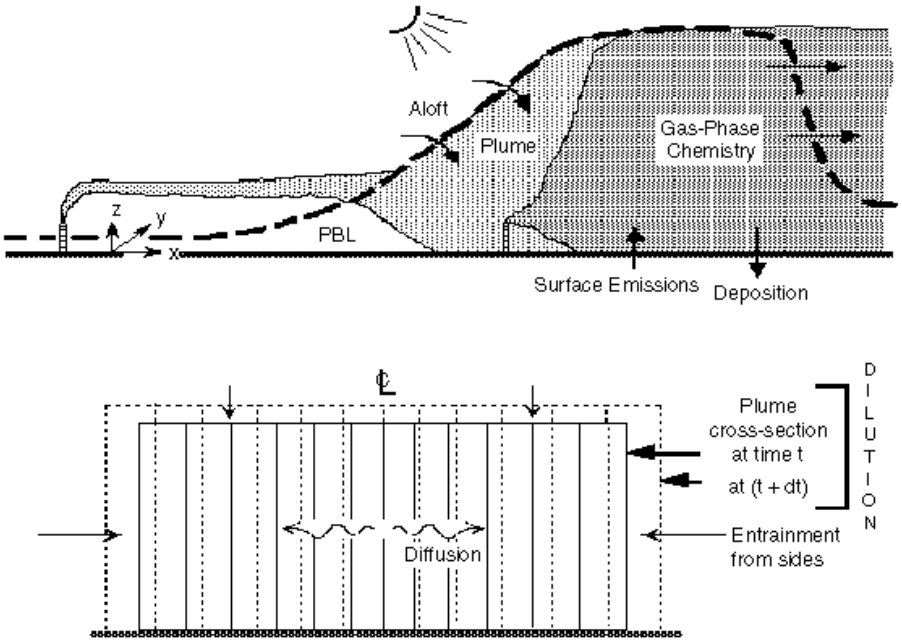

Figure 9-7. An illustration of the PinG module formulation depicting the relevant processes; a) time-height view and b) cross-sectional view.

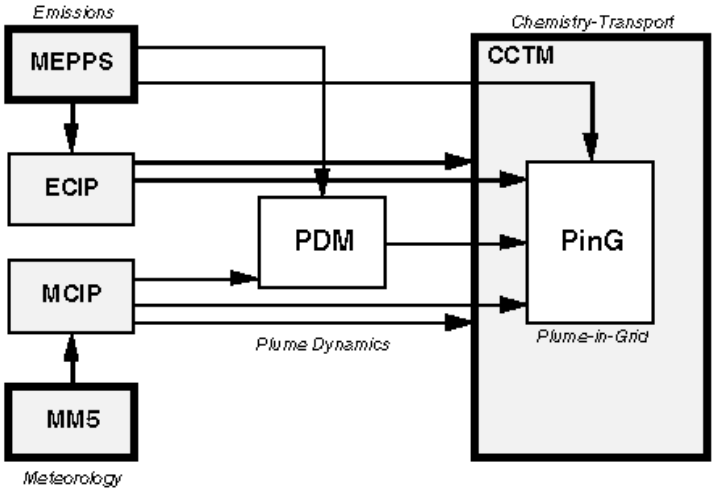

Figure 9-8. Flow diagram of the PDM processor and PinG module with associated programs in the Models-3 CMAQ system.

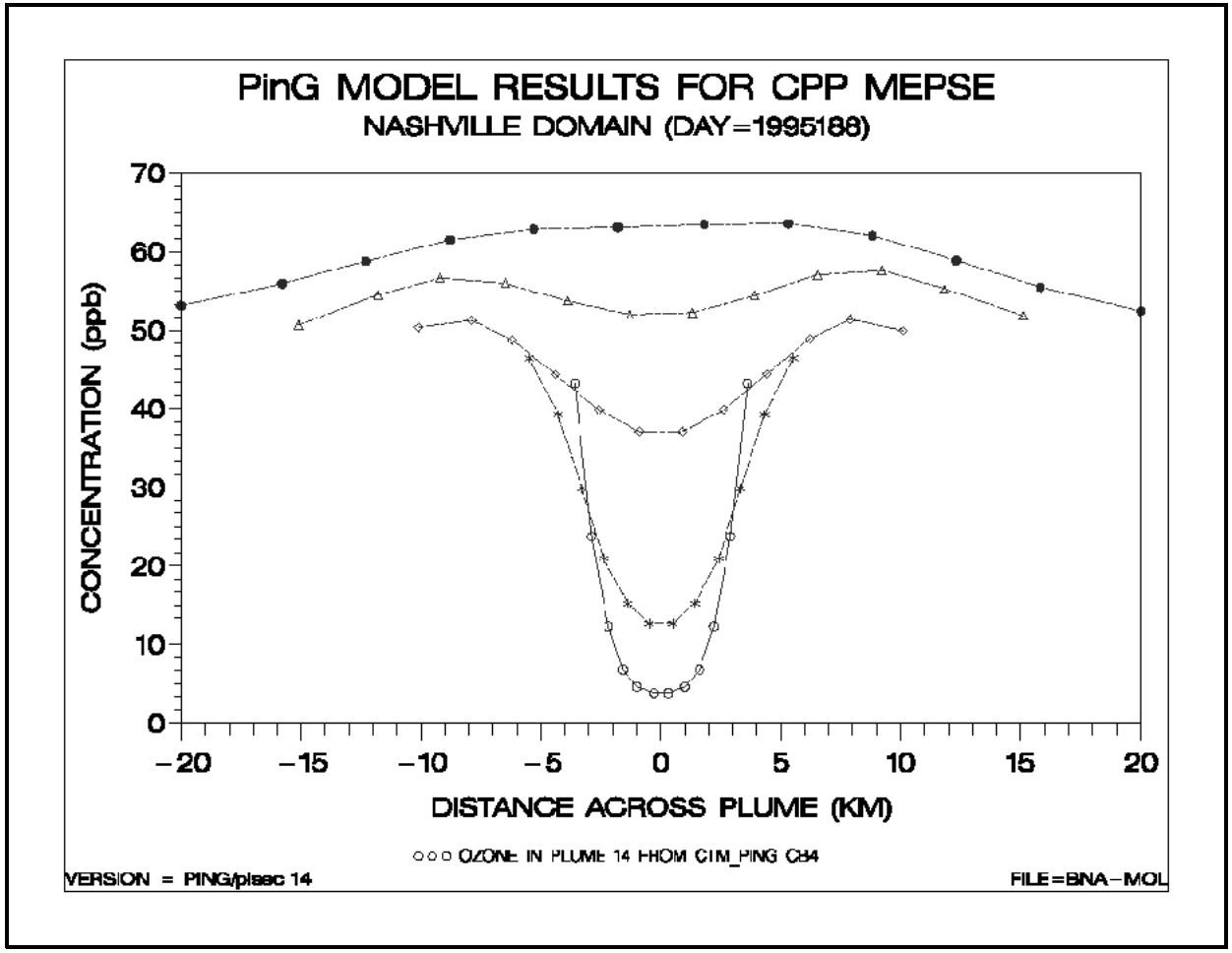

Figure 9-9 Plume ozone concentrations in an expanding cross-section in the subgrid scale plume phase at various times (o - 14:00, * - 14:30, ♢ - 15:30, △ - 15:30, • - 17:30). Plume section was released at 13:00. Symbol at each edge is the grid boundary concentration.